Editors' Suggestion

Thermodynamics and heat transport of a $Yb_3Sc_2Ga_3O_{12}$ single crystal: A quantum spin liquid candidate

Y. F. Xin,[1,*] A. Rutherford,[2,*] N. Li,[1,†] M. L. Feng,[1] Y. J. Liu,[1] Z. Y. Zhao,[1] Y. Y. Wang,[1] H. Liang,[1] Y. Zhou,[1] Q. J. Li,[3] M. Y. Xu,[4] W. Xie,[4] E. S. Choi,[5] X. Zhao,[6] J. Ma,[7] H. D. Zhou,[2,‡] and X. F. Sun[1,§]

[1]*Anhui Provincial Key Laboratory of Magnetic Functional Materials and Devices, Institutes of Physical Science and Information Technology, Anhui University, Hefei, Anhui 230601, People's Republic of China*

[2]*Department of Physics and Astronomy, University of Tennessee, Knoxville, Tennessee 37996, USA*

[3]*School of Physics and Optoelectronics, Anhui University, Hefei, Anhui 230061, People's Republic of China*

[4]*Department of Chemistry, Michigan State University, East Lansing, Michigan 48824, USA*

[5]*National High Magnetic Field Laboratory, Florida State University, Tallahassee, Florida 32310-3706, USA*

[6]*School of Physical Sciences, University of Science and Technology of China, Hefei, Anhui 230026, People's Republic of China*

[7]*Key Laboratory of Artificial Structures and Quantum Control, Shenyang National Laboratory for Materials Science, School of Physics and Astronomy, Shanghai Jiao Tong University, Shanghai 200240, People's Republic of China*

(Received 21 October 2025; accepted 6 January 2026; published 27 January 2026)

High-quality single crystals of $Yb_3Sc_2Ga_3O_{12}$ with a hyperkagome spin lattice were grown by using the floating-zone method. The magnetic susceptibility, specific heat and thermal conductivity were measured down to very low temperatures (<100 mK) to characterize the magnetic properties and probe the nature of ground state. The experimental results demonstrate that the ground state is spin disordered one with effective 1/2 spin and antiferromagnetic coupling, pointing to a possible quantum spin liquid, although the clear characteristic behaviors of quantum spin liquid were not observed in these results. The specific heat data display broad peaklike feature that is likely caused by the short-range spin correlations. The ultralow-temperature thermal conductivity exhibits rather strong magnetic field dependence and zero residual term (κ_0/T), which indicates the scattering between phonons and magnetic excitations. In addition, both the specific heat and thermal conductivity data display some field-induced magnetic transitions.

DOI: 10.1103/styt-544l

I. INTRODUCTION

Exploring novel states of matter driven by strong quantum fluctuations and competing interactions in spin frustrated systems has become one of the hotspots in the field of condensed matter physics. In conventional magnets, the interplay between spin exchange interactions and thermal fluctuations usually leads to long-range magnetic ordering (ferromagnetism or antiferromagnetism) at low temperatures, accompanied with the symmetry breaking in the systems. However, in some frustrated magnetic systems, this conventional long-range ordering can be suppressed even at absolute zero Kelvin. This leads to an intriguing, highly spin-entangled disordered quantum state called the quantum spin liquid (QSL). In a QSL, spins maintain strong correlations and continue to fluctuate by quantum mechanism, rather than fixing into an ordered pattern. QSLs are often characterized by exotic fractionalized excitations, including spinons, Majorana fermions, and topological visons, fundamentally different from spin waves in conventional magnets. These special elementary excitations are closely related to quantum computation and the microscopic origin of high temperature superconductivity [1–4], leading to significant attention on the investigation of QSL materials.

Theoretical exploration for QSLs was proposed on the two-dimensional (2D) triangular lattice by Anderson in 1973 [5]. After that, the realization of QSL materials was primarily focused on 2D systems. The representative examples of 2D QSL candidates are the triangular lattice antiferromagnets κ-$(BEDT\text{-}TTF)_2Cu_2(CN)_3$, $EtMe_3Sb[Pd(dmit)_2]_2$, $YbMgGaO_4$, $ARCh_2$ (A = alkali or monovalent ions, R = rare earth ions, Ch = chalcogenides), etc. [6–9] and the kagome lattice Herbertsmithite $ZnCu_3(OH)_6Cl_2$ and $Ca_{10}Cr_7O_{28}$ [10,11]. The other 2D honeycomb lattice materials $\alpha-RuCl_3$ and $Na_2Co_2TeO_6$ were found to have magnetic field induced QSL [12,13]. Moreover, quasi-one-dimensional antiferromagnet also exhibits the QSL state, such as the spin ladders and alternating spin chains [14], which is reasonable because low dimensionality and small spins enhance the low-energy quantum fluctuations and favor disordered ground states. Nevertheless, QSL can also be achieved in three-dimensional (3D) systems, especially in pyrochlore oxides of $A_2B_2O_7$ (A is a rare-earth ion and B is generally a nonmagnetic transition-metal ion) [15]. In this family, the existence of the dipole octupole doublets can support an exotic ground state of U(1) QSL, such as the newly discovered QSL state in the Ce-based

*These authors contributed equally to this work.
†Contact author: nli@ahu.edu.cn
‡Contact author: hzhou10@utk.edu
§Contact author: xfsun@ahu.edu.cn

TABLE I. The crystal structure and refinement of $Yb_3Sc_2Ga_3O_{12}$ at room temperature (Mo Kα radiation). Values in parentheses are estimated standard deviations from refinement.

Chemical formula	$Yb_3Sc_2Ga_3O_{12}$
Formula weight	1010.20 g/mol
Space Group	$Ia{-}3d$
Unit cell dimensions	$a = 12.362(8)$ Å
	$b = 12.362(8)$ Å
	$c = 12.362(8)$ Å
Volume	1889.51(6) Å^3
Z	8
Density (calculated)	7.102g/cm^3
Absorption coefficient	39.254 mm^{-1}
$F(000)$	3528.0
2θ range	8.076 to 81.912°
Reflections collected	2414
Independent reflections	520[$R_{\text{int}} = 0.0328$]
Refinement method	Full-matrix least-squares on F^2
Data/restraints/parameters	520/0/17
Final R indices	R_1 ($I > 2\sigma(I)$) = 0.0242; wR_2 ($I > 2\sigma(I)$) = 0.0632
	R_1(all) = 0.0307; wR_2 (all) = 0.0664
Largest diff. peak and hole	+7.76e/Å^3 and −1.77 e/Å^3
R. M. S. deviation from mean	0.505e/Å^3
Goodness-of-fit on F^2	1.125

pyrochlores [16,17]. Another famous example is the quantum spin ice state, which is actually also a U(1) QSL, has been proposed for $Tb_2Ti_2O_7$ and $Pr_2X_2O_7$ (X = Ir, Hf, Zr) [18–23].

In contrast to the extensive attentions on pyrochlore QSL, the hyperkagome lattice, a 3D network consisting of corner-sharing triangles, was found earlier to have possible QSL but has been less developed. Recently, with the enrichment of characterization methods, researchers revealed the rich ground state properties in this geometrically frustrated systems, such as QSL and classical spin liquid [24,25]. A promising result for the QSL ground state was reported for a hyperkagome material $PbCuTe_2O_6$ by using various low-temperature physical property measurement methods, such as muon spin relaxation, nuclear magnetic resonance and inelastic neutron scattering [26–28]. More recently, a hyperkagome lattice-based garnet $Yb_3Sc_2Ga_3O_{12}$ was reported to have a dynamic liquidlike ground state at least down to 130 mK, based on magnetic susceptibility and specific heat results on polycrystal samples [29], which is exceptional for $R_3Sc_2Ga_3O_{12}$ (R = rare earth) that mostly undergo a long-range antiferromagnetic ordering at low temperatures [30]. It would be interesting to identify the ground state of this material by carrying out detailed experimental characterizations on single-crystal samples.

Several experimental hallmarks have been widely accepted as evidence for QSL, including (i) a broad continuous magnetic intensity in the inelastic neutron scattering spectrum [10,31,32]; (ii) a large magnetic specific heat with power law ($C \sim T^{\alpha}$) temperature dependence [33–35]; and (iii) a nonzero residual thermal conductivity κ_0/T in the zero-Kelvin limit [3,36–40]. In this work, we grew high-quality $Yb_3Sc_2Ga_3O_{12}$ single crystals by using floating-zone method and measured magnetic susceptibility, specific heat and thermal conductivity down to very low temperatures. The experimental results clearly demonstrate a disordered ground state but do not display the above characteristic behaviors of QSL. The specific heat data are dominant by the short-range spin correlations at low temperatures, while the absence of residual thermal conductivity may be due to the scattering between phonons and magnetic excitations.

II. EXPERIMENTS

Single crystals of $Yb_3Sc_2Ga_3O_{12}$ were grown by using optical floating-zone method. One obtained single-crystal rod of $Yb_3Sc_2Ga_3O_{12}$ with good appearance is shown in

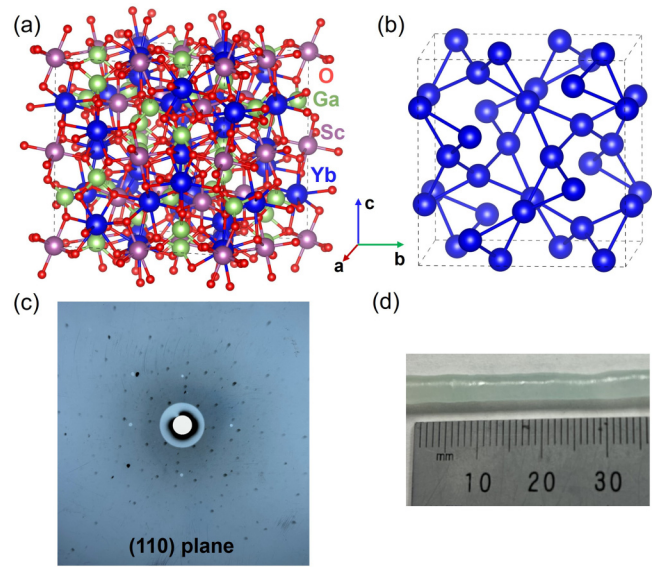

FIG. 1. (a) The crystal structure of $Yb_3Sc_2Ga_3O_{12}$ viewed along the c axis. (b) The hyperkagome networks formed by Yb^{3+} ions. (c) X-ray Laue back diffraction photo of the (110) plane. (d) The image of $Yb_3Sc_2Ga_3O_{12}$ single crystal grown by floating-zone method.

TABLE II. Atomic coordinates and equivalent isotropic atomic displacement parameters (Å^2) of $Yb_3Sc_2Ga_3O_{12}$.

$Yb_3Sc_2Ga_3O_{12}$	Wyck	x	y	z	Occ.	Uiso
Yb	24*c*	1/8	0	1/4	1	0.0030(1)
Sc	16*a*	0	0	0	1	0.000(2)
Ga	24*d*	3/8	0	1/4	1	0.0030(1)
O	96*h*	0.09534(17)	0.19015(18)	0.27733(18)	1	0.0040(3)

Fig. 1(d). The crystals were checked by x-ray diffraction and Laue photos, for which the good crystallinity can be confirmed by the sharp diffraction pattern, as shown in Fig. 1(c). The single crystal x-ray diffraction (SCXRD) measurement was performed using a XtalLAB Synergy, Dualflex, Hypix single crystal x-ray diffractometer with Mo K_α radiation ($\lambda = 0.71073$ Å). The structure was solved and refined using the Bruker SHELXTL Software Package. The refinement of the SCXRD data confirms the crystal structure of $Yb_3Sc_2Ga_3O_{12}$ with Yb^{3+} ions forming the hyperkagome networks, as shown in Figs. 1(a) and 1(b). The refinement results are listed in Tables I and II. The refinement of SCXRD data is consistent with the published powder XRD refinement [29], indicating the absence of site disorder of nonmagnetic ions in $Yb_3Sc_2Ga_3O_{12}$, which is different from some previously reported 2D magnetic materials with site mixture between different ions [8,10].

The dc magnetic susceptibility between 1.8 and 300 K were measured using the SQUID-VSM (Quantum Design Magnetic Property Measurement System, MPMS) in magnetic field up to 7 T. The dc magnetic susceptibility between 0.4 and 4 K were measured using the superconducting quantum interference device-vibrating sample magnetometer equipped with a ^{3}He refrigerator. The ac susceptibility with temperature down to 50 mK was measured using the conventional mutual inductance technique (with a combination of ac current source and a lockin amplifier) at SCM1 dilution fridge magnet of the National High Magnetic Field Laboratory, Tallahassee [41]. The specific heat was measured by a conventional relaxation method in the Physical Property Measurement System (PPMS, Quantum Design) with dilution insert down to 60 mK. The $Yb_3Sc_2Ga_3O_{12}$ single crystal for thermal conductivity measurements was cut and polished into a rectangular parallelepiped shape with longest direction and the largest surface in the (111) plane after being oriented by using the x-ray Laue system. Thus, the heat current was along the (111) plane, while the external magnetic fields were applied along ($B \perp$ [111]) or perpendicular to ($B \parallel$ [111]) the heat current. The thermal conductivity was measured in a ^{3}He/^{4}He dilution refrigerator (70 mK $< T <$ 1 K) equipped with a 14 T magnet, using the "one heater, two thermometers" technique [39,40].

III. RESULTS

Figures 2(a) and 2(c) show the temperature dependence of magnetic susceptibility χ measured with $B = 0.1$ T along or perpendicular to the [111] direction. The $\chi(T)$ increases upon lowering temperature and there is no visible anomaly down to 1.8 K, indicating the absence of long-range magnetic order. In addition, the field-cooling and zero-field-cooling susceptibility data does not show detectable difference, ruling out the possibilities of ferromagnetic moments or spin freezing down to 1.8 K. The inverse susceptibility show T-linear behavior at either high- or low-temperature range. The Curie-Weiss fit to the low-temperature data gives effective moment $\mu_{\text{eff}} = 1.763\ \mu_B$, Curie-Weiss temperature $\theta_{CW} = -0.31$ K for $B \parallel$ [111] and $\mu_{\text{eff}} = 1.764\ \mu_B$, $\theta_{CW} = -0.20$ K for $B \perp$ [111], respectively. Figures 2(b) and 2(d) show the isothermal magnetization curves at different temperatures from 1.8 to 15 K with the external magnetic fields along or perpendicular to the [111] direction. The $M(B)$ curves exhibit weak anisotropy and no field-induced transitions under the external fields up to 7 T for these two field directions. These results are in good agreement with those of polycrystal samples [29].

Figure 3(a) shows the dc magnetic susceptibility down to 0.4 K with $B \parallel$ [111] for $Yb_3Sc_2Ga_3O_{12}$ single crystal. Figure 3(b) shows the ac susceptibility down to 50 mK. It can be seen that the magnetic susceptibility continues to increase as the temperature decreases without any anomalies, which is different from the case of spin glass. One signature of spin glasses is a pronounced peak in $\chi'(T)$ curves and the freezing temperature T_f (defined as the peak temperature) is

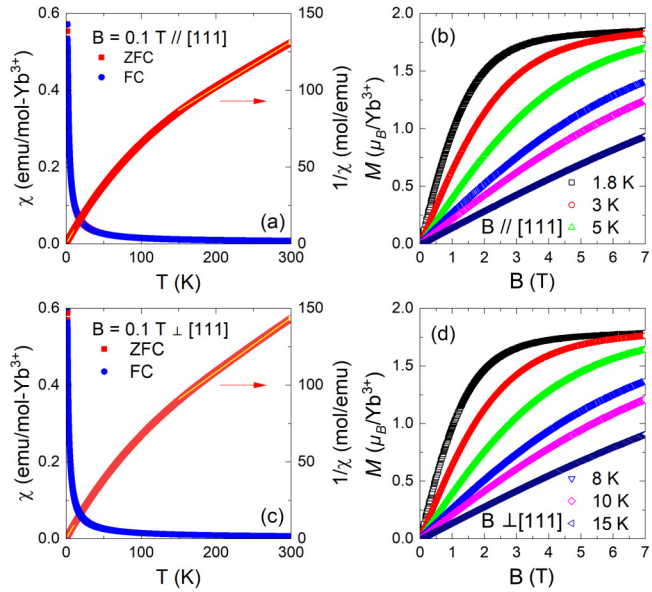

FIG. 2. (a), (c) Temperature dependence of dc magnetic susceptibility and the inverse magnetic susceptibility under zero-field cooling and field cooling of $Yb_3Sc_2Ga_3O_{12}$ single crystal for B (0.1 T) along or perpendicular to the [111] direction. The solid lines indicate the conventional Curie-Weiss fits to the high- and low-temperature ranges, respectively. (b), (d) The magnetization $M(B)$ curves of $Yb_3Sc_2Ga_3O_{12}$ single crystal at different temperatures with the external magnetic fields along or perpendicular to the [111] direction.

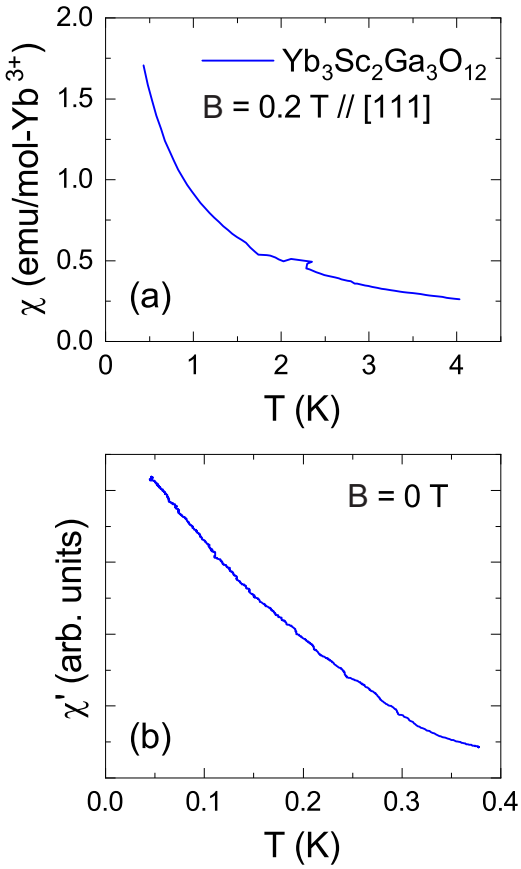

FIG. 3. (a) Dc magnetic susceptibility down to 0.4 K with $B \parallel [111]$ for $Yb_3Sc_2Ga_3O_{12}$ single crystal. (b) Ultralow-temperature ac susceptibility.

dependent on frequency [42]. The absence of broad peak in $\chi'(T)$ curve of $Yb_3Sc_2Ga_3O_{12}$ clearly indicates that there is no magnetic ordering or spin freezing at low temperatures down to 50 mK. All above magnetic property results demonstrate that $Yb_3Sc_2Ga_3O_{12}$ has a spin disordered ground state with antiferromagnetic correlation, which could be a QSL.

Figures 4(a) and 4(b) show the low-temperature specific heat of $Yb_3Sc_2Ga_3O_{12}$ single crystal in zero and different magnetic fields. These data indicate that in zero field there is no phase transition at low temperatures down to 60 mK, which again demonstrates the disordered ground state of this material. This is consistent with the results of magnetic susceptibility. At very low temperatures, the zero-field data show a broad peak that gradually moves to higher temperatures with increasing the external magnetic fields, which seems to be a Schottky behavior. However, it is notable that the magnitude of peak continuously increases with increasing field, which is remarkably different to the usual behavior of Schottky anomaly. The previous study on polycrystal sample has discovered similar low-temperature broad peak of specific heat [29]. Actually, although that work tried to fit this peak using a two-level Schottky formula, it pointed out the strong deviation of the zero-field data from the Schottky specific heat. This indicates that the low-temperature peak of specific heat is more likely due to the presence of short-range spin correlations between Yb^{3+} ions.

Since the magnetic contributions to the specific heat are significant only at very low temperatures, one can fit the phonon specific heat for the zero-field data at $T > 15$ K. It is known that in the temperature range $0.02 < T/\Theta_D < 0.1$ (Θ_D is the Debye temperature), one can use the low-frequency expansion of the Debye function, $C = \beta T^3 + \beta_5 T^5 + \beta_7 T^7$, where β, β_5 and β_7 are temperature-independent coefficients [43]. It should be noted that the use of polynomial functions to extract phonon specific heat is one useful method for specific heat data at not very high temperatures and has been effectively used for many magnetic materials [44–47]. As shown in Fig. 4(a), this formula gives a good fitting to the experimental data, with the parameters $\beta = 4.76 \times 10^{-4}\,\mathrm{J/K^4\,mol}$, $\beta_5 = 2.52 \times 10^{-7}\,\mathrm{J/K^6\,mol}$ and $\beta_7 = -1.43 \times 10^{-10}\,\mathrm{J/K^8\,mol}$. At very low temperatures, the T^5 and T^7 terms are negligible and the phonon specific heat has a well-known T^3 dependence with the coefficient of β. The inset to Fig. 4(a) shows the change of magnetic entropy below 10 K, S_m, calculated by integrating C_p/T (where the phonon specific heat is very small). The obtained entropy with applying magnetic fields are approaching the value of $R\ln 2$, with R is the universal gas constant. This indicates that $Yb_3Sc_2Ga_3O_{12}$ can be treated as an effective spin-1/2 system. It is notable that the zero-field entropy seems to saturate at about 4.5 J/mol K, which suggests the existence of residual entropy at very low temperatures. This is likely due to the persistent spin fluctuations caused by the frustration effect.

Figure 4(c) shows the magnetic field dependence of specific heat at 0.7 K with external magnetic field along the [111] direction. It displays a strong peak at 0.8 T, which suggests some kind of magnetic field induced transition. This phenomenon was not observed in the previous study on polycrystal sample [29]. Considering that the magnetization curves at $T \geqslant 1.8$ K do not exhibit any field-induced transition, this 0.8 T transition is likely a characteristic behavior emerged at very low temperatures. Figure 4(d) shows the ultralow-temperature specific heat under different magnetic fields along the [111] direction. There are two main features of these data. First, upon increasing magnetic field a small broad peak appears at the lowest temperatures, and this peak gradually moves to higher temperature accompanied with decreasing the peak magnitude. These behaviors can be well understood as the nuclear Schottky anomaly of Yb^{3+} ions. Second, a kinklike transition appears at about 0.2 K when the field arrives 1.8 T. This transition continuously moves to higher temperature but becomes weaker with further increasing magnetic field and finally becomes indiscernible for fields above 2.75 T. This result also points to some field-induced magnetic transitions.

Figure 5(a) shows the temperature dependence of thermal conductivity for $Yb_3Sc_2Ga_3O_{12}$ single crystal in zero field and in 14 T magnetic field along or perpendicular to the [111] direction. As one can see, the zero-field $\kappa(T)$ curve exhibits a $T^{2.8}$ power law behavior at very low temperatures, which is quite close to the standard phonon ballistic transport behavior (T^3dependence) [48]. The slight deviation can be due to either the phonon specular reflection effect or the existence of phonon scattering by magnetic excitations, which, in principle, can be identified by the effects of applying magnetic

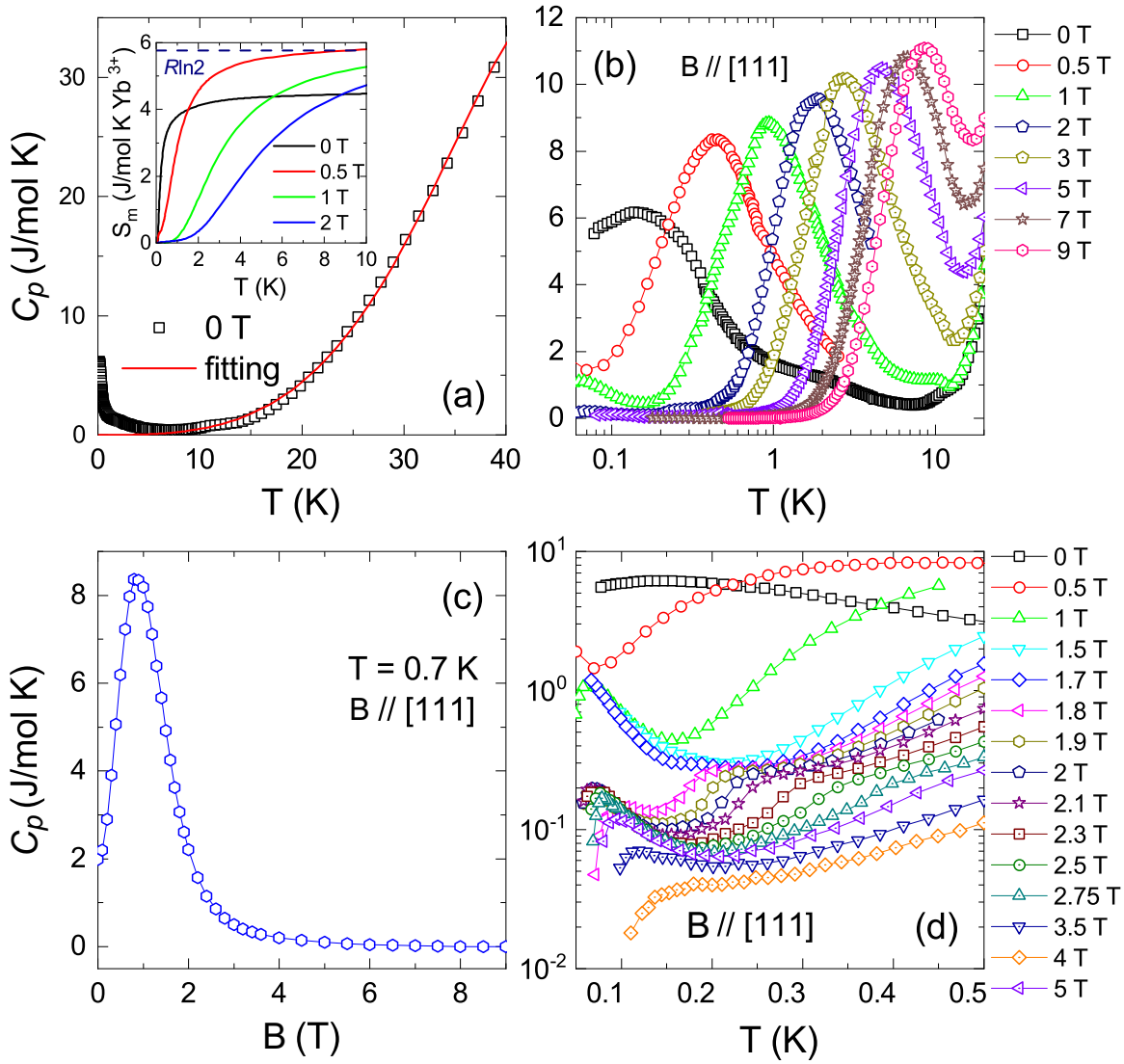

FIG. 4. (a) Specific heat $C_p(T)$ of $Yb_3Sc_2Ga_3O_{12}$ single crystal in zero field. The solid line is the fitting of phononic specific heat. Inset: the magnetic entropy at different magnetic fields. (b) Low-temperature specific heat under different magnetic fields along the [111] direction. (c) Field dependence of specific heat at $T = 0.7$ K. (d) Ultralow-temperature specific heat under different magnetic fields along the [111] direction.

field on thermal conductivity. Actually, 14 T field along or perpendicular to the [111] direction enhances the thermal conductivity in the whole temperature range from several tens mK to 1 K, which indicates the existence of phonon scattering by magnetic excitations in zero field. In addition, 14 T field along these two directions has almost the same effect on changing thermal conductivity.

It is useful to estimate the mean free path of phonons at low temperatures. The phononic thermal conductivity can be expressed by the kinetic formula $\kappa_{ph} = \frac{1}{3}Cv_pl$ [48], where $C = \beta T^3$ is phonon specific heat at low temperatures, v_p is the average velocity and l is the mean free path of phonon. Here $\beta = 4.76 \times 10^{-4}\,\mathrm{J/K^4\,mol}$ is obtained from the zero-field specific-heat data and $v_p = 2360$ m/s can be calulated from Deybe temperature Θ_D using the relations $\beta = \frac{12\pi^4}{5}\frac{Rs}{\Theta_D^3}$ and $\Theta_D = \frac{\hbar v_p}{k_B}(\frac{6\pi^2 Ns}{V})^{\frac{1}{3}}$ [43], where N is the number of molecules per mole and each molecule comprises s atoms, V is the volume of crystal and R is the universal gas constant. The inset to Fig. 5(b) shows the ratio of calculated l to the averaged sample width $W = 2\sqrt{A/\pi} = 0.323$ mm [48,49], where A is the area of cross section. It can be seen that the ratio l/W increases with lowering temperature and is about 0.6 at the lowest temperature, which means that the boundary scattering limit is not established at such low temperatures. It should be noted that these phonon mean free paths would be overestimated if there were sizable contribution to κ from other heat carriers. This result may exclude the surface reflection effect since the mean free path does not exceed the averaged sample width even at the lowest temperature.

Figure 5(b) shows the ultralow-temperature thermal conductivity at zero field. Many recent experimental studies revealed that the low-temperature thermal conductivity of gapless QSL candidates can be described by the formula of $\kappa/T = \kappa_0/T + bT^{\alpha-1}$, where κ_0/T represents a constant contribution from gapless fermionic excitations and bT^{α}

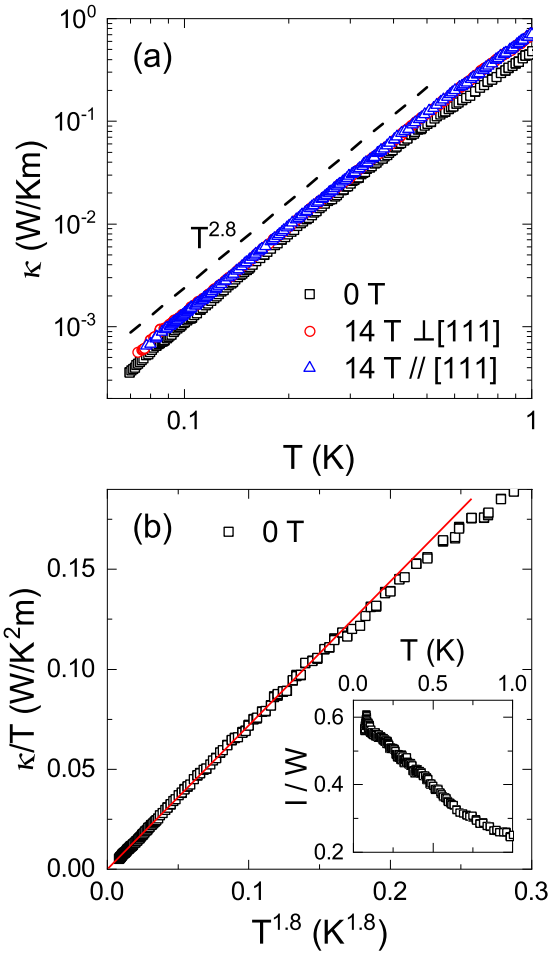

FIG. 5. (a) Temperature dependence of the thermal conductivity measured at zero field and 14 T-field applied along or perpendicular to the [111] direction. (b) Zero-field thermal conductivity plotted in κ/T vs $T^{1.8}$. The solid line represents the linear fitting. The inset shows the temperature dependence of the phonon mean free path l divided by the averaged sample width W.

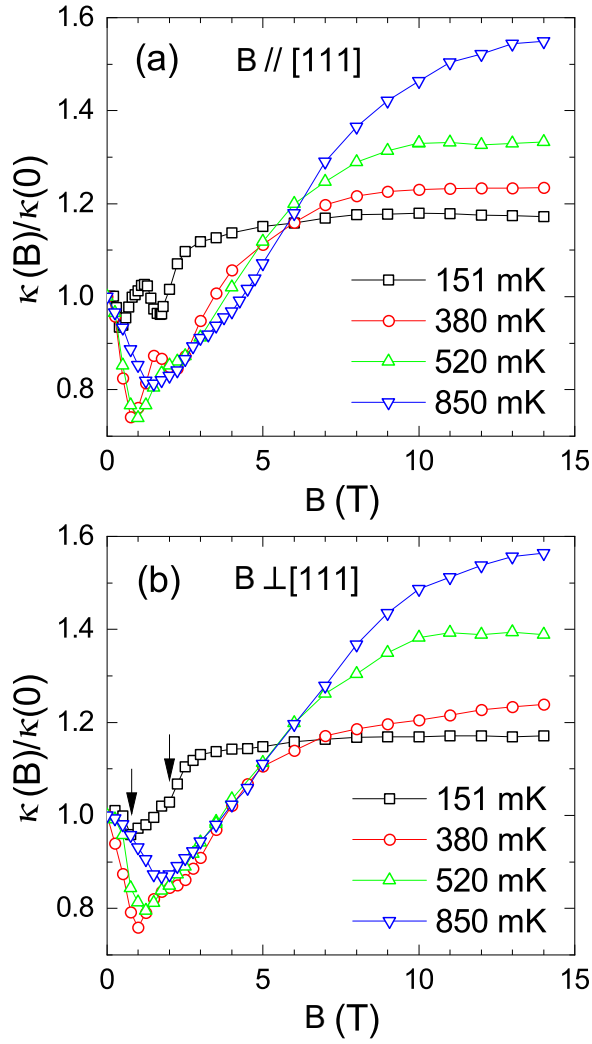

FIG. 6. Isothermal thermal conductivity as a function of the magnetic field for fields applied along or perpendicular to the [111] direction.

represents the phonon thermal conductivity with the exponent $\alpha = 2 \sim 3$ [3,38–40]. As shown in Fig. 5(b), the linear fitting at $T < 350$ mK gives a zero residual thermal conductivity, κ_0/T. Moreover, the larger κ in high fields indicates that at zero field the phonons are scattered by magnetic excitations, which are gapped out in high magnetic fields. Therefore, the absence of magnetic contribution to the thermal conductivity result at zero field is due to the spin-phonon scattering that not only weakens the phonon transport but also prevents the spinon transport. This result is very similar to that of some other QSL candidates, such as $PrMgAl_{11}O_{19}$ [50], $NaYbS_2$, and $NaYbSe_2$ [51].

Figure 6 shows the magnetic field dependence of thermal conductivity at different temperatures with external magnetic field along or perpendicular to the [111] direction. For $B \parallel$ [111], the $\kappa(B)/\kappa(0)$ isotherm at $T = 151$ mK displays two clear dips at 0.75 and 1.75 T and saturates at high fields with a weak increase (∼18%). With increasing temperature, the two dips become weaker and moves to higher fields, while the high-field increase of κ becomes larger without saturation. The data for $B \perp$ [111] are very similar. In particular, the high field values of thermal conductivity are almost the same for the two field directions, which are consistent with the nearly isotropic magnetic properties revealed by the magnetization results. The only one difference is that the dips are weaker for $B \perp$ [111]. The dips of $\kappa(B)$ indicate two magnetic transitions since a minimum of thermal conductivity most likely results from the strong scattering of phonons by magnetic fluctuations at the critical point [52–56]. Similar phenomenon has been observed in the QSL candidates $Na_2BaCo(PO_4)_2$ and $YbMgGaO_4$ [39,40] and $NaYbCh_2$ ($Ch =$ S, Se) [51], in which the magnetic field-induced transitions are related to the arrangement of the spin structure. This result further indicates that the ground state of $Yb_3Sc_2Ga_3O_{12}$ is likely a quantum spin liquid rather than a paramagnetic one.

IV. DISCUSSIONS

Both the magnetic susceptibility and specific heat data measured down to several tens mK indicate absence of long-range magnetic ordering and spin freezing in

$Yb_3Sc_2Ga_3O_{12}$ single crystals. Since Yb^{3+} ions have been found to have effective 1/2 spin and antiferromagnetic coupling, it is very likely that this material is a QSL candidate. But why were the characteristic behaviors of QSL not observed in thermodynamic and transport results? First, most 2D gapless QSL candidates display power-law temperature dependence of magnetic specific heat at very low temperatures, while $Yb_3Sc_2Ga_3O_{12}$ show a dominant feature of broad peak or hump due to the short-range spin correlations. It is similar to the result of 3D QSL candidate $Tb_2Ti_2O_7$ [57,58]. Second, the itinerant gapless spinons in QSL are expected to contribute to the thermal conductivity, which yields a nonzero residual term κ_0/T at $T \rightarrow 0$ K [7,39,40]. It has become the smoking gun of the itinerant spinons and gapless QSL. However, the absence of κ_0/T was observed at zero-Kelvin limit in the present work. Based on the magnetic field dependence of κ, it is likely that there are low-energy spinons scattering with phonons. It should be pointed out that in many QSL candidates, there is rather strong coupling between phonons and spinons, which leads to weak temperature dependence of ultralow-temperature κ and rather small κ_0/T contributed by the spinon transport [40,50,51]. Thus, although the present experiments display the absence of κ_0/T at zero field, the $\kappa(T)$ and $\kappa(B)$ data actually indicate the existence of spinons that scatter with phonons. This possibility has been found recently in some other QSL candidate, $PrMgAl_{11}O_{19}$ [50], $NaYbS_2$, and $NaYbSe_2$ [51]. Third, both the specific heat and thermal conductivity data indicate the field-induced magnetic transitions. Similar phenomena have also been found in some other QSL candidates [39,40]. Although the mechanisms of these transitions remained to be investigated, they demonstrate that the disordered ground state is likely a QSL rather than a simple paramagnetic one. Therefore, the present experimental results on high-quality single crystal seem to suggest that $Yb_3Sc_2Ga_3O_{12}$ is a 3D QSL candidate. Since the present thermodynamic and transport results do not give direct support to the QSL, further experimental investigations, particularly on the magnetic excitation spectrum, are called for.

V. SUMMARY

In this work, we grew high-quality single crystals of hyperkagome system $Yb_3Sc_2Ga_3O_{12}$ and characterized magnetic properties and ground state by using the measurements of magnetic susceptibility, specific heat and thermal conductivity measurements at very low temperatures. On one hand, the experimental results demonstrate that the ground state is spin disordered one with antiferromagnetic coupling, pointing to a possible QSL. On the other hand, all these results, however, do not exhibit the clear characteristic behaviors of QSL. The specific heat data display a broad peaklike feature that is likely caused by the short-range spin correlations. The ultralow-temperature thermal conductivity exhibits rather strong magnetic field dependence and zero residual term κ_0/T, which indicates the scattering between phonons and magnetic excitations. Furthermore, the specific heat and thermal conductivity data indicate some magnetic-field induced transitions.

ACKNOWLEDGMENTS

This work was supported by the National Key Research and Development Program of China (Grant No. 2023YFA1406500), the National Natural Science Foundation of China (Grants No. 12404043, No. 12574042, No. 12274388, and No. 12204004), and the Nature Science Foundation of Anhui Province (Grant No. 2408085QA024). The work at the University of Tennessee was supported by the NSF with Grant No. NSF-DMR-2003117. M.Y.X. and W.X. are supported by the U.S. DOE-BES under Contract No. DE-SC0023648. A portion of this work was performed at the National High Magnetic Field Laboratory, which is supported by National Science Foundation Cooperative Agreement No. DMR-2128556* and the State of Florida and the U.S. Department of Energy.

DATA AVAILABILITY

The data that support the findings of this article are not publicly available. The data are available from the authors upon reasonable request.

[1] A. Y. Kitaev, Fault-tolerant quantum computation by anyons, Ann. Phys. **303**, 2 (2003).

[2] A. Kitaev, Anyons in an exactly solved model and beyond, Ann. Phys. **321**, 2 (2006).

[3] P. W. Anderson, The resonating valence bond state in La_2CuO_4 and superconductivity, Science **235**, 1196 (1987).

[4] P. A. Lee, N. Nagaosa, and X.-G. Wen, Doping a Mott insulator: Physics of high-temperature superconductivity, Rev. Mod. Phys. **78**, 17 (2006).

[5] P. W. Anderson, Resonating valence bonds: A new kind of insulator? Mater. Res. Bull. **8**, 153 (1973).

[6] B. Miksch, A. Pustogow, M. J. Rahim, A. A. Bardin, K. Kanoda, J. A. Schlueter, R. Hübner, M. Scheffler, and M. Dresse, Gapped magnetic ground state in quantum spin liquid candidate κ-$(BEDT\text{-}TTF)_2Cu_2(CN)_3$, Science **372**, 276 (2021).

[7] M. Yamashita, N. Nakata, Y. Senshu, M. Nagata, H. M. Yamamoto, R. Kato, T. Shibauchi, and Y. Matsuda, Highly mobile gapless excitations in a two-dimensional candidate quantum spin liquid, Science **328**, 1246 (2010).

[8] Y. Li, H. Liao, Z. Zhang, S. Li, F. Jin, L. Ling, L. Zhang, Y. Zou, L. Pi, Z. Yang, J. Wang, Z. Wu, and Q. Zhang, Gapless quantum spin liquid ground state in the two-dimensional spin-1/2 triangular antiferromagnet $YbMgGaO_4$, Sci. Rep. **5**, 16419 (2015).

[9] W. Liu, Z. Zhang, J. Ji, Y. Liu, J. Li, X. Wang, H. Lei, G. Chen, and Q. Zhang, Rare-earth chalcogenides: A large family of triangular lattice spin liquid candidates, Chin. Phys. Lett. **35**, 117501 (2018).

[10] T.-H. Han, J. S. Helton, S. Chu, D. G. Nocera, J. A. Rodriguez-Rivera, C. Broholm, and Y. S. Lee, Fractionalized excitations in the spin-liquid state of a kagome-lattice antiferromagnet, Nature (London) **492**, 406 (2012).

[11] C. Balz, B. Lake, J. Reuther, H. Luetkens, R. Schönemann, T. Herrmannsdörfer, Y. Singh, A. T. M. N. Islam, E. M. Wheeler,

J. A. Rodriguez-Rivera, T. Guidi, G. G. Simeoni, C. Baines, and H. Ryll, Physical realization of a quantum spin liquid based on a novel frustration mechanism, Nat. Phys. **12**, 942 (2016).

[12] S.-H. Do, S.-Y. Park, J. Yoshitake, J. Nasu, Y. Motome, Y. S. Kwon, D. T. Adroja, D. J. Voneshen, K. Kim, T.-H. Jang, J.-H. Park, K.-Y. Choi, and S. Ji, Majorana fermions in the Kitaev quantum spin system $\alpha-RuCl_3$, Nat. Phys. **13**, 1079 (2017).

[13] G. Lin, J. Jeong, C. Kim, Y. Wang, Q. Huang, T. Masuda, S. Asai, S. Itoh, G. Günther, M. Russina, Z. Lu, J. Sheng, L. Wang, J. Wang, G. Wang, Q. Ren, C. Xi, W. Tong, L. Ling, Z. Liu, *et al.*, Field-induced quantum spin disordered state in spin-1/2 honeycomb magnet $Na_2Co_2TeO_6$, Nat. Commun. **12**, 5559 (2021).

[14] Y. Zhou, Quantum spin liquid states, Rev. Mod. Phys. **89**, 025003 (2017).

[15] J. S. Gardner, M. J. P. Gingras, and J. E. Greedan, Magnetic pyrochlore oxides, Rev. Mod. Phys. **82**, 53 (2010).

[16] Y.-D. Li and G. Chen, Symmetry enriched U(1) topological orders for dipole-octupole doublets on a pyrochlore lattice, Phys. Rev. B **95**, 041106(R) (2017).

[17] E. M. Smith, O. Benton, D. R. Yahne, B. Placke, R. Schäfer, J. Gaudet, J. Dudemaine, A. Fitterman, J. Beare, A. R. Wildes, S. Bhattacharya, T. DeLazzer, C. R. C. Buhariwalla, N. P. Butch, R. Movshovich, J. D. Garrett, C. A. Marjerrison, J. P. Clancy, E. Kermarrec, G. M. Luke, *et al.*, Case for a $U(1)_\pi$ quantum spin liquid ground state in the dipole-octupole pyrochlore $Ce_2Zr_2O_7$, Phys. Rev. X **12**, 021015 (2022).

[18] H. R. Molavian, M. J. P. Gingras, and B. Canals, Dynamically induced frustration as a route to a quantum spin ice state in $Tb_2Ti_2O_7$ via virtual crystal field excitations and quantum many-body effects, Phys. Rev. Lett. **98**, 157204 (2007).

[19] L. Yin, J. S. Xia, Y. Takano, N. S. Sullivan, Q. J. Li, and X. F. Sun, Low-temperature low-field phases of the pyrochlore quantum magnet $Tb_2Ti_2O_7$, Phys. Rev. Lett. **110**, 137201 (2013).

[20] G. Chen, "Magnetic monopole" condensation of the pyrochlore ice U(1) quantum spin liquid: Application to $Pr_2Ir_2O_7$ and $Yb_2Ti_2O_7$, Phys. Rev. B **94**, 205107 (2016).

[21] V. K. Anand, L. Opherden, J. Xu, D. T. Adroja, A. T. M. N. Islam, T. Herrmannsdorfer, J. Hornung, R. Schonemann, M. Uhlarz, H. C. Walker, N. Casati, and B. Lake, Physical properties of the candidate quantum spin-ice system $Pr_2Hf_2O_7$, Phys. Rev. B **94**, 144415 (2016).

[22] K. Kimura, S. Nakatsuji, J.-J. Wen, C. Broholm, M. B. Stone, E. Nishibori, and H. Sawa, Quantum fluctuations in spin-icelike $Pr_2Zr_2O_7$, Nat. Commun. **4**, 1934 (2013).

[23] S. Petit, E. Lhotel, S. Guitteny, O. Florea, J. Robert, P. Bonville, I. Mirebeau, J. Ollivier, H. Mutka, E. Ressouche, C. Decorse, M. C. Hatnean, and G. Balakrishnan, Antiferroquadrupolar correlations in the quantum spin ice candidate $Pr_2Zr_2O_7$, Phys. Rev. B **94**, 165153 (2016).

[24] M. J. Lawler, H.-Y. Kee, Y. B. Kim, and A. Vishwanath, Topological spin liquid on the hyperkagome lattice of $Na_4Ir_3O_8$, Phys. Rev. Lett. **100**, 227201 (2008).

[25] J. A. M. Paddison, H. Jacobsen, O. A. Petrenko, M. T. Fernández-Díaz, P. P. Deen, and A. L. Goodwin, Hidden order in spin-liquid $Gd_3Ga_5O_{12}$, Science **350**, 179 (2015).

[26] B. Koteswararao, R. Kumar, P. Khuntia, S. Bhowal, S. K. Panda, M. R. Rahman, A. V. Mahajan, I. Dasgupta, M. Baenitz, K. H. Kim, and F. C. Chou, Magnetic properties and heat capacity of the three-dimensional frustrated $S = 1/2$ antiferromagnet $PbCuTe_2O_6$, Phys. Rev. B **90**, 035141 (2014).

[27] P. Khuntia, F. Bert, P. Mendels, B. Koteswararao, A. V. Mahajan, M. Baenitz, F. C. Chou, C. Baines, A. Amato, and Y. Furukawa, Spin liquid state in the 3D frustrated antiferromagnet $PbCuTe_2O_6$: NMR and muon spin relaxation studies, Phys. Rev. Lett. **116**, 107203 (2016).

[28] S. Chillal, Y. Iqbal, H. O. Jeschke, J. A. Rodriguez-Rivera, R. Bewley, P. Manuel, D. Khalyavin, P. Steffens, R. Thomale, A. T. M. N. Islam, J. Reuther, and B. Lake, Evidence for a three-dimensional quantum spin liquid in $PbCuTe_2O_6$, Nat. Commun. **11**, 2348 (2020).

[29] B. Sana, M. Barik, M. Pregelj, U. Jena, M. Baenitz, J. Sichelschmidt, K. Sethupathi, and P. Khuntia, Magnetic properties of a spin-orbit entangled $J_{\text{eff}} = 1/2$ three-dimensional frustrated rare-earth hyperkagome material, Phys. Rev. B **108**, 134413 (2023).

[30] P. Mukherjee, A. C. S. Hamilton, H. F. J. Glass, and S. E. Dutton, Sensitivity of magnetic properties to chemical pressure in lanthanide garnets $Ln_3A_2X_3O_{12}$, Ln = Gd, Tb, Dy, Ho, A = Ga, Sc, In, Te, X = Ga, Al, Li, J. Phys.: Condens. Matter **29**, 405808 (2017).

[31] Y. Shen, Y.-D. Li, H. Wo, Y. Li, S. Shen, B. Pan, Q. Wang, H. C. Walker, P. Steffens, M. Boehm, Y. Hao, D. L. Quintero-Castro, L. W. Harriger, M. D. Frontzek, L. Hao, S. Meng, Q. Zhang, G. Chen, and J. Zhao, Evidence for a spinon Fermi surface in a triangular-lattice quantum-spin-liquid candidate, Nature (London) **540**, 559 (2016).

[32] J. A. M. Paddison, M. Daum, Z. Dun, G. Ehlers, Y. Liu, M. B. Stone, H. Zhou, and M. Mourigal, Continuous excitations of the triangular-lattice quantum spin liquid $YbMgGaO_4$, Nat. Phys. **13**, 117 (2017).

[33] S. Yamashita, Y. Nakazawa, M. Oguni, Y. Oshima, H. Nojiri, Y. Shimizu, K. Miyagawa, and K. Kanoda, Thermodynamic properties of a spin-1/2 spin-liquid state in a κ-type organic salt, Nat. Phys. **4**, 459 (2008).

[34] O. I. Motrunich, Variational study of triangular lattice spin-1/2 model with ring exchanges and spin liquid state in κ-$(ET)_2Cu_2(CN)_3$, Phys. Rev. B **72**, 045105 (2005).

[35] S. S. Lee and P. A. Lee, U(1) gauge theory of the Hubbard model: Spin liquid states and possible application to κ-$(BEDT\text{-}TTF)_2Cu_2(CN)_3$, Phys. Rev. Lett. **95**, 036403 (2005).

[36] C. P. Nave and P. A. Lee, Transport properties of a spinon Fermi surface coupled to a U(1) gauge field, Phys. Rev. B **76**, 235124 (2007).

[37] Y. Werman, S. Chatterjee, S. C. Morampudi, and E. Berg, Signatures of fractionalization in spin liquids from interlayer thermal transport, Phys. Rev. X **8**, 031064 (2018).

[38] M. Yamashita, Boundary-limited and glassylike phonon thermal conduction in $EtMe_3$ $Sb[Pd(dmit)_2]_2$, J. Phys. Soc. Jpn. **88**, 083702 (2019).

[39] N. Li, Q. Huang, X. Y. Yue, W. J. Chu, Q. Chen, E. S. Choi, X. Zhao, H. D. Zhou, and X. F. Sun, Possible itinerant excitations and quantum spin state transitions in the effective spin-1/2 triangular-lattice antiferromagnet Na_2 $BaCo(PO_4)_2$, Nat. Commun. **11**, 4216 (2020).

[40] X. Rao, G. Hussain, Q. Huang, W. J. Chu, N. Li, X. Zhao, Z. Dun, E. S. Choi, T. Asaba, L. Chen, L. Li, X. Y. Yue, N. N.

Wang, J.-G. Cheng, Y. H. Gao, Y. Shen, J. Zhao, G. Chen, H. D. Zhou, and X. F. Sun, Survival of itinerant excitations and quantum spin state transitions in $YbMgGaO_4$ with chemical disorder, Nat. Commun. **12**, 4949 (2021).

[41] Z. L. Dun, M. Lee, E. S. Choi, A. M. Hallas, C. R. Wiebe, J. S. Gardner, E. Arrighi, R. S. Freitas, A. M. Arevalo-Lopez, J. P. Attfield, H. D. Zhou, and J. G. Cheng, Chemical pressure effects on magnetism in the quantum spin liquid candidates $Yb_2X_2O_7$ (X = Sn, Ti, Ge), Phys. Rev. B **89**, 064401 (2014).

[42] J. A. Mydosh, *Spin Glasses: An Experimental Introduction* (Taylor Francis, London, 1993).

[43] A. Tari, *Specific Heat of Matter at Low Temperatures* (Imperial College Press, London, 2003).

[44] T. Lancaster, S. J. Blundell, M. L. Brooks, P. J. Baker, F. L. Pratt, J. L. Manson, M. M. Conner, F. Xiao, C. P. Landee, F. A. Chaves, S. Soriano, M. A. Novak, T. P. Papageorgiou, A. D. Bianchi, T. Herrmannsdörfer, J. Wosnitza, and J. A. Schlueter, Magnetic order in the $S = 1/2$ two-dimensional molecular antiferromagnet copper pyrazine perchlorate $Cu(Pz)_2(ClO_4)_2$, Phys. Rev. B **75**, 094421 (2007).

[45] Z. Y. Zhao, X. M. Wang, C. Fan, W. Tao, X. G. Liu, W. P. Ke, F. B. Zhang, X. Zhao, and X. F. Sun, Magnetic phase transitions and magnetoelectric coupling of $GdFeO_3$ single crystals probed by low-temperature heat transport, Phys. Rev. B **83**, 014414 (2011).

[46] R. Nath, M. Padmanabhan, S. Baby, A. Thirumurugan, D. Ehlers, M. Hemmida, H.-A. K. von Nidda, and A. A. Tsirlin, Quasi-two-dimensional $S = 1/2$ magnetism of $Cu[C_6H_2(COO)_4][C_2H_5NH_3]_2$, Phys. Rev. B **91**, 054409 (2015).

[47] S. Guchhait, R. Kolay, A. Magar, and R. Nath, Magnetic and crystal electric field studies of two Yb^{3+}-based triangular lattice antiferromagnets, arXiv:2501.14590.

[48] R. Berman, *Thermal Conduction in Solids* (Oxford University Press, Oxford, 1976).

[49] X. F. Sun and Y. Ando, Comment on "Low-temperature phonon thermal conductivity of single-crystalline Nd_2CuO_4: Effects of sample size and surface roughness", Phys. Rev. B **79**, 176501 (2009).

[50] N. Li, A. Rutherford, Y. Y. Wang, H. Liang, Q. J. Li, Z. J. Zhang, H. Wang, W. Xie, H. D. Zhou, and X. F. Sun, Ising-type quantum spin liquid state in $PrMgAl_{11}O_{19}$, Phys. Rev. B **110**, 134401 (2024).

[51] N. Li, M. T. Xie, Q. Huang, Z. W. Zhuo, Z. Zhang, E. S. Choi, Y. Y. Wang, H. Liang, Y. Sun, D. D. Wu, Q. J. Li, H. D. Zhou, G. Chen, X. Zhao, Q. M. Zhang, and X. F. Sun, Thermodynamics and heat transport in the quantum spin liquid candidates $NaYbS_2$ and $NaYbSe_2$, Phys. Rev. B **110**, 224414 (2024).

[52] S. Guang, N. Li, R. L. Luo, Q. Huang, Y. Wang, X. Yue, K. Xia, Q. Li, X. Zhao, G. Chen, H. Zhou, and X. Sun, Thermal transport of fractionalized antiferromagnetic and field-induced states in the Kitaev material $Na_2Co_2TeO_6$, Phys. Rev. B **107**, 184423 (2023).

[53] N. Li, Q. Huang, A. Brassington, X. Y. Yue, W. J. Chu, S. K. Guang, X. H. Zhou, P. Gao, E. X. Feng, H. B. Cao, E. S. Choi, Y. Sun, Q. J. Li, X. Zhao, H. D. Zhou, and X. F. Sun, Quantum spin state transitions in the spin-1 equilateral triangular lattice antiferromagnet $Na_2BaNi(PO_4)_2$, Phys. Rev. B **104**, 104403 (2021).

[54] X. Zhao, Z. Y. Zhao, L. M. Chen, X. Rao, H. L. Che, L. G. Chu, H. D. Zhou, L. S. Ling, J. F. Wang, and X. F. Sun, Frustration-free spatially anisotropic $S = 1$ square-lattice antiferromagnet $Ni[SC(NH_2)_2]_6Br_2$, Phys. Rev. B **99**, 104419 (2019).

[55] J. D. Song, X. M. Wang, Z. Y. Zhao, J. C. Wu, J. Y. Zhao, X. G. Liu, X. Zhao, and X. F. Sun, Low-temperature heat transport of $CuFe_{1-x}Ga_xO_2$ (x = 0-0.12) single crystals, Phys. Rev. B **95**, 224419 (2017).

[56] X. M. Wang, C. Fan, Z. Y. Zhao, W. Tao, X. G. Liu, W. P. Ke, X. Zhao, and X. F. Sun, Large magnetothermal conductivity of $HoMnO_3$ single crystals and its relation to the magnetic-field-induced transitions of magnetic structure, Phys. Rev. B **82**, 094405 (2010).

[57] M. J. P. Gingras, B. C. den Hertog, M. Faucher, J. S. Gardner, S. R. Dunsiger, L. J. Chang, B. D. Gaulin, N. P. Raju, and J. E. Greedan, Thermodynamic and single-ion properties of Tb^{3+} within the collective paramagnetic-spin liquid state of the frustrated pyrochlore antiferromagnet $Tb_2Ti_2O_7$, Phys. Rev. B **62**, 6496 (2000).

[58] Q. J. Li, Z. Y. Zhao, C. Fan, F. B. Zhang, H. D. Zhou, X. Zhao, and X. F. Sun, Phononglasslike behavior of magnetic origin in single-crystal $Tb_2Ti_2O_7$, Phys. Rev. B **87**, 214408 (2013).